Energy & Buildings 358 (2026) 117208

Contents lists available at ScienceDirect

Energy & Buildings

journal homepage: www.elsevier.com/locate/enb

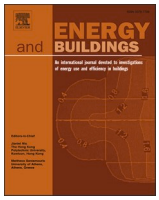

Integrating seismic and energy retrofits in built heritage: timber-based solutions within the "nested building" approach☆

Matteo Salvalaggio [a,b,1], Laura Carnieletto [c,*], Elisa Saler [d], Wilmer Pasut [c], Umberto Turrini [e], Maria Rosa Valluzzi [a]

[a] Department of Cultural Heritage, University of Padova, piazza Capitaniato 7, 35139 Padova, Italy
[b] Institute for Sustainability and Innovation in Structures Engineering (ISISE), ARISE, Department of Civil Engineering, University of Minho, Guimarães, Portugal
[c] Department of Environmental Sciences, Informatics and Statistics, Ca' Foscari University of Venice, Dorsoduro, 3246, 30123 Venice, Italy
[d] Department of Geosciences, University of Padova, via G. Gradenigo 6, 35131 Padova, Italy
[e] Department of Civil, Environmental and Architectural Engineering, University of Padova, via Marzolo 9, 35131 Padova, Italy

ARTICLE INFO

Keywords:
Seismic retrofit
Energy retrofit
Integrated intervention
Energy scenarios
Cross-Laminated Timber CLT
Heritage masonry

ABSTRACT

Ensuring the long-term preservation of the built heritage addresses two key aspects: the safeguard against natural hazards like earthquakes and the update of performances to contemporary standards.

The paper discusses the use of the *Nested Building* retrofit technique, aiming to achieve an integrated refurbishment strategy for existing masonry buildings, by introducing a Cross-Laminated Timber endoskeleton designed to update structural, thermal, and functional performances. The study discusses the application of this technique to a heritage building, adopted as a pilot case. The capability of *Nested Building* in integrating seismic and thermal enhancement was assessed by employing global numerical simulations. Seismic strengthening was evaluated through non-linear static analyses in a finite element environment, whilst the energy savings were computed through a dynamic energy simulation tool. A range of layouts was explored, implementing incremental levels of strengthening and insulation.

The study revealed the effectiveness of *Nested Building* technique in integrating the seismic and thermal retrofit of masonry buildings. Notably, even when applied to a specific portion of the building system, the intervention still provides valuable improvements.

1. Introduction

The Italian and European building standards has evolved over centuries in parallel with advancements in technology and increases in society wealth. However, the major part of European built heritage is nowadays dated, with 31% built before 1945, 20% between 1945 and 1965, while 28% dates to the new millennium [1]. The most of this stock does not meet safety, energy efficiency and comfort standards, due to a persistently low renovation rate [2].

The safety level of these dated buildings is further exacerbated when exposed to seismic actions. In the Italian area, one of the most prone to earthquake, 60% of the building stock was built before first seismic regulation in 1974, while 88% before the first energy provision in 1991 [3,4]. Additionally, buildings often underwent alterations that may compromise their load-bearing capacity. For example, reinforced concrete (RC) components combined with poor-quality masonry and inadequate connections were found to negatively affect seismic performance [5–7]. This highlights the need to enhance the seismic capacity of the built heritage that does not comply with regulatory standards, also reversing the effects of previous improper structural interventions.

Moreover, the global built environment accounts for approximately 49% of worldwide CO_2 emissions, with 21% attributed to materials and 28% to operational activities [8]. In the European area (European Union and United Kingdom), the building stock is responsible for the 40% of

☆ This article is part of a special issue entitled: 'Rethinking Resilience' published in Energy & Buildings.

* Corresponding author.
E-mail addresses: matteo.salvalaggio@civil.uminho.pt, matteo.salvalaggio@epfl.ch (M. Salvalaggio), laura.carnieletto@unive.it (L. Carnieletto), elisa.saler@unipd.it (E. Saler), wilmer.pasut@unive.it (W. Pasut), umberto.turrini@unipd.it (U. Turrini), mariarosa.valluzzi@unipd.it (M.R. Valluzzi).
[1] Present address: Ecolé Polytechnique Fédérale de Lausanne (EPFL), Earthquake Engineering and Structural Dynamics Laboratory (EESD), Lausanne, 1015, Switzerland.

https://doi.org/10.1016/j.enbuild.2026.117208
Received 10 May 2025; Received in revised form 30 January 2026; Accepted 20 February 2026
Available online 22 February 2026

total energy consumption [9]. In parallel, the continuous expansion of cities through new constructions and associated infrastructures – while obsolete buildings are often overlooked rather than addressed – contributes to the consumption of virgin land, thereby reducing the resilience of such environments to climate change. As a result, ensuring the sustainability of both building operations and construction practices has become a critical objective, which also led to the definition of the European Missions on Climate Adaptation and Climate-Neutral and Smart Cities.

Within this context – where structural safety, energy efficiency, and comfort need to be simultaneously addressed within building systems – integrated retrofit strategies have gained significant attention for their potential to deliver multi-performance improvements [10] while refurbishing obsolete building stocks. Most of these strategies embed structural performance within thermal insulation layers [2,11,12], or conversely integrate thermal performance within structural components [13,14]. Alternative solutions rely on separate yet coupled layers dedicated to structural strengthening and energy efficiency, forming double-skin retrofit systems or exoskeletons [15], particularly applied to RC structures [16–18]. While sectorial retrofit interventions can provide similar performance improvements, it has been shown that integrated interventions can enable further benefits [17]. They are capable of improving i) the economic sustainability by minimizing construction phase costs while exploiting synergies, ii) the environmental sustainability by minimizing the construction phase impacts (Global Warming Potential, Water usage and Waste production), and iii) the social sustainability, by reducing the downtime and inhabitant disturbance during construction [19].

Among integrated solutions, timber-based strategies stand out for their sustainability and potential for innovative applications, offering eco-friendly alternatives for the retrofit of existing buildings [20–23]. A broader discussion of the improvements in seismic capacity and energy efficiency achieved through the use of timber-based solutions is provided in Sub-Sections 1.1 and 1.2. Indeed, the traditional coupling of materials such as timber and load-bearing masonry has been recently explored by various authors to devise innovative and engineered retrofit strategies.

To tackle the dual challenge of improving structural safety and energy efficiency in URM buildings, the authors have proposed an integrated retrofit strategy known as *Nested Building* [21,24]. This approach couples existing masonry walls with Cross-Laminated Timber (CLT) components and incorporates dedicated insulation layers, aiming to enhance seismic performance, reduce thermal energy dispersion, and improve indoor comfort. A key feature of this strategy is the preservation of the building outer architectural identity, while allowing substantial internal transformations. The intervention entails the demolition of obsolete interior structural elements – such as walls, floors, and the roof – and the insertion of new insulation and load-bearing layers behind the façades, in the shape of an endoskeleton.

The concept of integration in this context serves a dual role: it refers both to the simultaneous improvement of structural and energy performance, and to the physical embedment of new systems within the existing fabric. Rooted in the principles – sustainability, aesthetics, and inclusion – of the New European Bauhaus, the *Nested Building* strategy is particularly suited for buildings with severely compromised performance, where reconstruction would otherwise be necessary or economically convenient, yet where preserving the external envelope maintains its cultural or architectural value [23,25,26].

While several studies have numerically assessed the retrofitting of URM structures with timber elements, most focus on structural aspects, or they are lumped at the component (local) scale. Full-scale simulations using Equivalent Frame Models have explored timber retrofit techniques [27,28], without specifically investigating the potential of CLT panels and their integration within URM structures through endoskeletons [23]. Other studies [24,29,30] investigated the structural and energy performance of URM-CLT coupling at the local scale (e.g., masonry piers), yet a comprehensive, building-scale assessment remains missing. This paper seeks to fill these gaps, providing an integrated analysis of seismic and energy performance improvements at the building scale using the *Nested Building* approach. Through the combination of detailed structural and energy modeling, various retrofit configurations are examined by crossing the impact of different endoskeleton layouts and envelope insulation strategies on primary energy demand and seismic capacity.

In this paper, the effectiveness of *Nested Building* as an integrated retrofit strategy was tested at global scale on a pilot case. This consists of a XVII-century heritage masonry building, *Cattedra*, in the North-East Italian Alpine Region, whose structural, thermal, and functional performances have become obsolete. Based on pier-scale coupled URM-CLT solutions for the improvement of structural [21,31,32] and hygrothermal performances [24,29], the intervention was here extended to the entire structure. Incremental structural and insulation interventions were simulated until the achievement of the full *Nested Building* layout. To overcome the limitations of deterministic analyses, this study incorporates the inherent variability of URM materials by adopting upper- and lower-bound values for mechanical properties, thereby capturing a representative range of structural responses.

The structural behavior of the pilot-case study and its retrofit configurations was assessed using the finite element method (FEM) [33], through quasi-static (pushover) analyses conducted in accordance with the Performance-Based Assessment (PBA) framework outlined in NTC2018 [34]. In parallel, space heating and cooling energy demands, at hourly timestep, were provided through EnergyPlus [35], a whole building energy simulation tool combined with the open-source suite Open Studio [36].

The results aim to demonstrate the potential of this approach as a viable solution for the sustainable refurbishment of historic masonry buildings. Using the pilot case as a reference, the study offers insights into the application of *Nested Building* concept as a retrofit strategy capable of integrating structural, thermal and functional improvements in existing masonry buildings. By addressing structural and thermal needs within a single intervention, this approach may also reduce construction time and overall costs through the integration of shared operations and labour. Additionally, the study quantifies the benefits of partial intervention strategies when a comprehensive approach is not feasible.

1.1. *On the use of timber components for the structural retrofit of masonry structures*

Recent studies have been focused on the design and testing of various structural retrofit techniques based on timber strong-backs or panels, whose advantages have been previously discussed by the authors [21]. A summary of key studies from the literature is provided in Table 1. In general, the coupling of URM walls with timber panels proved to be an effective strengthening strategy, yielding increases in both load (from + 20% to + 129%) and displacement (from 25% to 166%) capacities. The initial stiffness was found unaltered – compared to bare specimens – when distributed fasteners were used.

Novel insights were provided by the recent timber cladding system designed for the retrofit of Canadian masonry buildings [30], which provided a marked increase in displacement and ductility capacities, although a slight decrease of peak load was recorded.

1.2. *On the use of timber for the improvement of thermal performance*

Since the energy consumption of buildings is significantly related to the envelope characteristics, the choice of building materials is fundamental to achieve energy savings alongside with the pursuit of embedded CO_2 reduction measures and sustainability goals [42,43].

Shin et al. [44] calculated the effect on embodied energy and carbon reduction, as well as operational energy, achievable by replacing

Table 1
Main structural characteristics and experimental in-plane performance of URM piers coupled with timber retrofit layer.

Paper		Sustersic and Dujic 2014 [37]	Sustersic and Dujic 2014 [37]	Pozza, Evangelista, and Scotta 2017 [38]; Pozza et al. 2021 [32]	Borri, Sisti, and Corradi 2021 [39]	Giongo et al. 2021 [31]	Guerrini et al. 2021 [40]	Rizzi et al. 2022 [41]	Liu et al. 2025 [30]
Type of unreinforced masonry		Double-wythe Flemish bond clay brick	Double-wythe Flemish bond clay brick	Semi-hollow bricks	Calcareous stone masonry and sand-hydraulic lime mortar	340 mm-thick clay brick and lime mortar	Single-wythe running bond calcium silicate	Rubble stone and lime mortar	Double-wythe common bond clay brick
Type of timber retrofit		120 mm-thick three-layers CLT panel	120 mm-thick three-layers CLT panel	27 mm-thick three-layer solid wood panel	60 mm-thick three-layers CLT (one side) + steel wires repointing (Reticulatus) (one side)	60 mm-thick three-layers CLT	80 × 60 mm strong-backs + 18 mm thick-OSB panel connected via Ø4 × 75/100 mm anker nails	60 mm-thick three-layers CLT	38 × 90 mm lumber elements and plywood panel connected via Ø8 × 45 screws and polyurethane adhesive
Type of connection	**Lumped (top/bottom edges)**	Steel bolted lumped at edges	–	Timber screws (2 rows, 50 mm spacing)	–	Top ribbed steel plate pre-loaded with wires	Fastened within RC beams	–	–
	Distributed	–	Epoxy resin	–	9 × ∅8 mm steel bars	No. 17 Ø12 × 180; no. 16 or 25 Ø10 × 230 steel screws	Angle fasteners	5 x 8.8 grade threaded ∅14 mm anchors with epoxy resin	Chemically anchored ∅12.7 × 230 rods with custom spacing
Peak force [kN]	**Bare**	100	100	24	134.3	69.3; 75.9	78	22.02	237.5; 224.2
	Strengthened	134	134	55	267.26	95; 91.1; 106	105	29.82	188.1; 192.2
	Difference	+34%	+34%	+129%	+99%	+37%; +20%	+35%	+35%	−20.8%; −14.28%
Ultimate displacement [mm] / Drift [-]	**Bare**	10/0.6%	10/0.66%	28/2%	–	>40/ 2.2%; >50/ 2.7%	20.2/0.75%	–	0.29; 0.34 / 0.25‰; 0.28‰
	Strengthened	20/1.2%	12.5/0.8%	44/3.1%	–	>80/ 4.4%	54/2%	–	21.74; 22.99 / 1.81%; 1.9%
	Difference	+100%	+25%	+57%	–	–	+166%	–	+7396%; +6661%
Increase of initial stiffness		No	Yes	No	–	No (for R-3)	No	–	No

concrete and steel with CLT combined with various insulators. They estimated that using CLT to build 30% of the exterior walls of the potential 800′000 new dwellings in Seoul by 2030 could result in energy savings of up to 11′495 TJ and a greenhouse gas reduction of about 0.86 Mt CO_2 eq.

Furthermore, the use of CLT walls can enhance indoor comfort. Kang et al. [45] proposed a study with two approaches to achieve a comfortable indoor environment while reducing energy use. They applied passive and active technologies, replacing external walls with CLT and modifying the control temperature for space heating and cooling, validating the predictive simulations with on-site tests. Subsequently, the resulting changes in indoor hygrothermal environments and energy performance were analyzed, obtaining an increase of indoor air temperature by more than 1°C compared to that with the existing concrete wall and an energy reduction for space heating ranging from 5% to 16%, depending on the CLT technology applied. Since the literature widely demonstrated the impact of indoor comfort of occupants on building energy consumption, novel approaches should be studied to provide a desirable indoor environment limiting the operation of indoor heating, ventilation, and air conditioning (HVAC) systems or using heat recovery [46] to provide the desired indoor environment avoiding an increase of energy consumption [47]. For example, Myroniuk et al. [48] explored passive systems for regulating microclimates in residential settings, with a focus on modular constructions. In addition, the definition of construction details is of paramount importance for both the indoor comfort and the durability of the intervention. Thus, it is important to note that a vapor barrier and/or a breathable water-stop layer should always be included in the intervention layout to increase the durability of the timber [29].

2. Materials and methods

The Nested Building (NB) approach aims to refurbish existing buildings by introducing an internal endoskeleton coupled with the perimeter walls, while replacing obsolete inner components. This method enhances structural integrity, thermal performance, and energy efficiency, bringing the retrofitted building in line with current standards.

Among the conventional materials and solutions, the use of CLT panels emerges as the most balanced solution from the previous studies of the authors [21]. It can improve stiffness and strength with a limited increase, or even decrease, in masses. Nonetheless, load variations on URM walls should be carefully controlled, due to the positive correlation between shear strength and vertical compression stress.

In this study, the validation of the *Nested Building* as integrated strategy is carried out on a heritage building part of the *Cattedra* building system in Canove di Roana (Vicenza) (Section 3.1), assumed as a pilot case. The selected structure is representative of a large stock of heritage

masonry buildings lacking significant cultural or artistic value, which have undergone multiple structural alterations aimed solely at accommodating changing functional needs, ultimately compromising their structural and seismic performance while ignoring any energy-saving measures.

The investigations on integrated seismic-energy retrofit are based on FEM, in the DIANA FEA environment [33], while the software used for dynamic energy modelling is EnergyPlus [35].

Both structural and energy models were developed following an incremental retrofit approach, to assess the contribution of each component to the overall performance improvement. Moreover, alternative intervention layouts were considered, i.e., limited to the second and third floor, named Partial (P), or extended to the entire building, named Complete (C).

The systematic crossing of standalone energy and structural retrofit scenarios allows for the evaluation of their interaction and the identification of the optimal integrated strategy. The sectorial and integrated retrofit scenarios are anticipated in Table 2.

The layout of structural models are depicted in Fig. 1, namely, i) As-Built (AsB), the bare current configuration; ii) Floor Substitution (FS), where existing floors and roof are replaced with CLT ones; iii) Partial Nested Building intervention (NB-P), with the implementation of the endoskeleton and substitution of central URM wall with CLT panels, although limited to the second and third stories, with existing first floor unaltered; iv) Complete Nested Building (NB-C), with interventions implemented along the entire building height. Given the negligible structural influence of the energy retrofit layer, this was not considered in the structural models, resulting in comparatively less structural retrofit scenarios than those adopted for energy simulations.

The Energy Retrofit (ER) strategy consists of installing 10 cm of expanded polystyrene (EPS) within an insulated wall lining system finished with plasterboard, ensuring compliance with fire safety requirements. This solution is considered sufficient to achieve a significant energy performance of about 0.2 W/(m^2 K) while avoiding massive space reduction, with the replacement of existing windows. For comparison purposes, the performance of the bare timber endoskeleton (NBb), without the incorporation of the ER is also analyzed. The energy performance scenarios evaluated are then: the as-built scenario AsB, without any structural and energy improvement; two purely thermal retrofit (ER-P, ER-C) models; two purely structural retrofit layouts (NBb-P and NBb-C); two integrated scenarios (NB-P, NB-C). The structural and energy models constructed, based on the crossing between structural retrofit and insulation layers, are listed in Table 2.

Numerical structural simulations are based on 2-D shell elements, capable of accurate prediction of both historical masonry [49–51] and CLT [52,53] structures, and their coupling [54]. The capability of FEM to simulate the response of URM piers coupled with CLT panels was benchmarked against the outcomes of experimental tests carried out by Giongo et al. [31] on existing URM piers, consistent with the application of NB. Once validated the numerical strategy as described in Appendix A, full-scale FE model of the *Cattedra* case study was constructed.

Dynamic energy simulations for the various scenarios were carried out with the EnergyPlus software to evaluate the seasonal energy demand for space heating and cooling. Sub-Section 4.2 presents the energy performance results in terms of energy demand and primary energy consumption, considering the installation of different systems for space heating and cooling.

2.1. The pilot-case

Originally built in the XVII century, *Cattedra* had undergone several transformations over the years with the aim of maximizing its functionality and minimizing costs, regardless of its structural behavior, energy efficiency or historical value. Thereby, the height of the structure was increased by adding another story while traditional timber floors were replaced with cast-in-place RC joists ones.

The pilot-case (Fig. 2) is currently a three-story building in the North-East Italian Alpine region, with regular rectangular plan (10 x 13 m) and eave height 8.2 m. Longitudinal façades are parallel to North-South axis. East (Fig. 2a) and West (Fig. 2b) longitudinal façades have a regular layout of piers and lintels, due to aligned openings. A row of filled openings (i.e., the third one) runs along all façades. South façade (Fig. 2c) has three large piers and thin lintels, with only two windows still open. Horizontal structures consist of three diaphragms and a double-pitched roof. First and second floors are made of cast-in-place RC joists and clay blocks with slab, the third floor and the roof are made of clay block joists without RC slab (known in Italy as *SAP – Senza armatura provvisoria*). Therefore, the building lacks an effective roof diaphragm. Walls consist of an average 60 cm-thick (i.e., varying between 55 and 70 cm) double-wythe masonry made of white hewn stone (roughly cut stone), locally known as *biancone*, with a good average size of the units and a binder in a poor state of conservation. The two wythes rely on the presence of through-stones, while corner attachment is guaranteed by quoins. The height of the interface between the historical unit (stone masonry) and the additional story (modern 60 cm-thick hollow clay block masonry) was also detected at 7 m. Fig. 2d reports a structural scheme of the case study.

2.2. Structural modeling and design

The nonlinear behavior of masonry was simulated by a smeared approach, i.e., Total Strain Crack Model, embedded in DIANA code, which proved to be effective in URM static nonlinear analysis of heritage masonry [55,56]. The numerical methodology was first validated against the experimental investigations of Giongo et al. [31] on the behavior of coupled CLT-URM walls under lateral loads. A detailed description of the experimental benchmark and the validation procedure is reported in Appendix A.

Table 2
Summary of structural and dynamic energy models in function of retrofit scenarios.

Structural retrofit	Insulation layer	Structural model	Energy model	Description
None	None	AsB	AsB	As-Built baseline scenario.
Floor Substitution (CLT diaphragms)	None	FS	–	Structural stiffening of floor diaphragms scenario by substitution of existing cast-in-place RC floors with CLT ones.
None	Insulated wall lining system (10 cm EPS) and windows replacement	–	ER-P [a]; ER-C [a]	Sectorial energy retrofit scenario with application of thermal insulation.
Timber Endoskeleton	None	NB-P [a b]; NB-C [a b]	NBb-P [a]; NBb-C [a]	Sectorial structural retrofit scenario through construction of the bare timber endoskeleton, without dedicated thermal insulation.
Timber Endoskeleton	Insulated wall lining system (10 cm EPS) and windows replacement	NB-P [a]; NB-C [a]	NB-P [a]; NB-C [a]	Integrated retrofit scenario with timber endoskeleton associated with thermal insulation.

[a] = Partial retrofit layout restricted to 2nd and 3rd floors (−P); complete retrofit layout applied to the whole building (−C).
[b] = The influence of the EPS layer on structural performance is considered negligible. The outcomes of structural models for NB are valid whether thermal insulation is present or not.

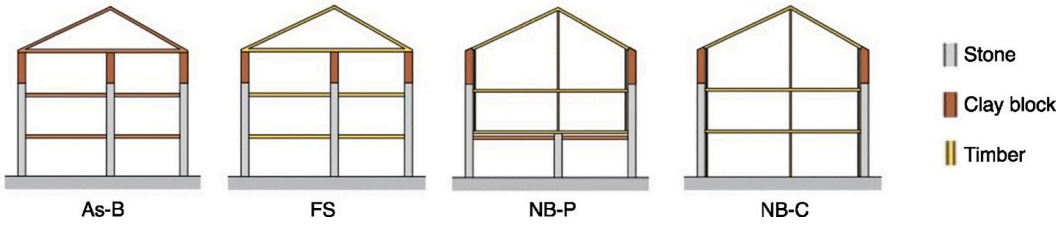

Fig. 1. Scheme of Nested building intervention for *Cattedra* pilot case: As-Built configuration (As-B); Floor Substitution (FS); Partial intervention limited to second and third floor (NB-P); Complete intervention involving the entire structure (NB-C).

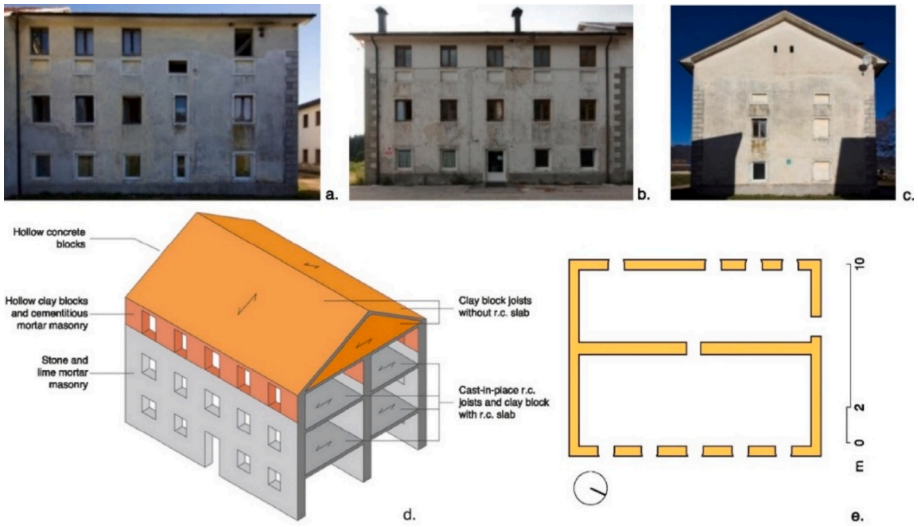

Fig. 2. "Cattedra" pilot case: a) East longitudinal façade [21], b) West longitudinal façade [21], c) South transverse façade [21], d) structural scheme, e) typological plan.

Compression was modeled by a parabolic compression law based on fracture energy, with values derived according to [33,56]. Tensile behavior was considered elastic until peak strength, whilst post peak was described through an exponential softening law governed by tensile fracture energy.

Density, Young's modulus E, shear modulus G, compressive strength f_c and initial shear strength (cohesion) τ values were adopted according to [57], reduced by a confidence factor (CF) of 1.35 to account for a limited knowledge level (KL1) according to [58]. Tensile strength f_t was derived from shear strength τ [59,60], as per Eq. (1).

$$f_t = 1.5\tau \tag{1}$$

Compressive fracture energies G_{fc} was derived through Eq. (2) discussed by [56,61].

$$G_{fc} = d \bullet f_c \tag{2}$$

where d is the ductility index assumed equal to 1 [56,61]. For tensile fracture energy G_{ft} and shear behavior, two sets of properties were defined to represent the lower (LB) and upper (UB) bound conditions. This was devised to address the marked sensitivity of URM modeling to these parameters (see Appendix A).

In relation to the LB properties, tensile fracture energy G_{ft} was derived according to Eq. (3) [56,61].

$$G_{ft} = 0.025(2f_t)^{0.7} \tag{3}$$

In addition, fixed shear crack orientation was assumed with a shear retention value β equal to 0.01 [55]. In relation to the UB properties, G_{ft} value was taken by [62]. Crack orientation was assumed to be rotating [63], as suggested in [62,64]. Table 3 summarizes the values adopted for masonry components.

Table 3
URM mechanical properties for the *Cattedra* structure in function of LB and UB sets.

	Hewn stone masonry		Semi-hollow clay block	
	LB	UB	LB	UB
E [MPa]	1740		4550	
ν [-]	0.25		0.25	
f_c [MPa]	1.12		1.85	
G_{fc}[N/mm]	3.01		4.84	
f_t [MPa]	0.018		0.037	
G_{ft} [N/mm]	0.00135	0.02	0.004	0.02
Crack orientation	Fixed	Rotating	Fixed	Rotating
β [-]	0.01	–	0.01	–
ρ [kg/m^3]	2000		1500	

Floors with RC slabs, in the AsB layout, were modeled using 5 cm-thick shells with bidirectional stiffness. Existing floors without slabs were considered ineffective (i.e., third floor and roof). Table 4 lists the values of mechanical parameters adopted for the floor diaphragms.

Floor masses (according to seismic combination of [34] and a live load of 200 kg/m^2) are lumped at wall-to-diaphragm intersection,

Table 4
Mechanical properties of RC floor diaphragms (AsB layout).

Property	Cast-In-Place RC Joists and Clay Blocks with Slab
Structural thickness (cm)	5
Young's modulus E_x (MPa)	20′000
Young's modulus E_y (MPa)	39′200
Shear modulus G_{xy} (MPa)	8′300

whereas URM walls and CLT panels masses are assumed distributed (i.e., implemented as material density). Models constructed are discretized through a 20 cm-size mesh. Fig. 3 illustrates the numerical models constructed.

Although the floors in NB retrofit configurations are connected to, and supported by, the masonry façades, it is essential that the CLT endoskeleton is capable of bearing both gravity and seismic loads in the event that URM components lose their structural capacity. The design of steel brackets and timber panels was done according to [65,66], based on response spectrum analysis with a behavior factor (q) equal to 2.5 and a medium ductility class (DCM). The seismic action considered is described in Sub-Section 3.2.1. Table 5 shows the characteristics of designed CLT panels and brackets.

CLT members (in the FS, NB-P and NB-C cases) were modeled according to the so-called component modeling approach [69]. Panels were discretized as orthotropic linear shells, according to [53,70], while nonlinear behavior was lumped at connection systems. Traditional steel brackets for timber were modeled assuming a tri-linear law based on producer testing reports [71]. Hold-down elements were modeled as point interface elements, with symmetrical laws in compression and tension; shear brackets as springs with shear laws. Panel-to-panel and panel-to-lintel shear interfaces were calibrated based on experimental push-out tests [72], assuming zero stress and stiffness after failure. Table 6 lists the properties of CLT panels according to producer data [73].

Table 5
Characteristics of connectors and CLT elements at each floor, according to the NB-P and NB-C interventions.

Layout		Floor	Steel brackets [67,68]			
			Longitudinal		Transverse	
			Hold-down	Angle-bracket	Hold-down	Angle-bracket
NB-C		F0	16 × WHT440 12 × WHT540	17 × TTN240	20 × WHT540	13 × TTN240
	NB-P	F1	28 × WHT440	17 × TTN240	20 × WHT540	13 × TTN240
		F2	28 × WHT340	8 × TTN240	10 × WHT340	16 × TTN240

Layout		Element	CLT panels Material	No. of layers	Thickness [mm]	Layers [mm]
NB-C	NB-P	Wall	Spruce C24	3	100	30 – 40 – 30
		First floor	Spruce C24	5	160	40 – 20 – 40 – 20 – 40
		Second floor	Spruce C24	5	140	40 – 20 – 20 – 20 – 40
		Roof	Spruce C24	3	100	30 – 40 – 30

2.2.1. Characterization of seismic demand and assessment procedure

The pilot case arises in the Italian Alpine region, in the municipality of Roana, with a moderate seismicity (ground acceleration for 475-years return period at bedrock is equal to 0.142 g). The seismic demand for the area is characterized according to [34] for the Serviceability Limit State, i.e., Operational Limit State (OLS), Damage Limitation Limit State (DLS), and Ultimate limit states, i.e., Life-Safety Limit State (LLS) and Near-Collapse Limit State (CLS). Ground type B, topographic category T2 (average slope $> 15°$) and reference life period of 50 years were assumed. Fig. 4 reports the main seismic spectra in function of limit states.

The seismic capacity of the retrofit scenarios was assessed according PBA and N2 method [74]. Although Capacity Spectrum method could be considered more suitable for masonry structures [75], N2 method was adopted since incorporated in the Italian and European guidelines [34,66].

2.3. Dynamic energy model

The detailed energy model of the building was carried out combining the Open Studio [36] interface with the software for dynamic simulations Energy Plus [35]. Each floor was divided into thermal zones based on the assigned use of the space, and then internal loads associated with the presence of people, lighting and office electrical equipment were assigned. EN 16798: 2019 standard [76] was used to define the sensible load fraction due to the presence of people – 70 W/person – and the occupancy schedule of a working day, as presented in Fig. 5.

The contributions of lighting and electrical equipment (computers, printers, etc.) was adopted according to [77], i.e., 3 W/m^2 for specific light loads and 4 W/m^2 for appliances. Sensible loads related to people are implemented by splitting the contribution as 60% radiative and 40% convective, while equipment loads are equally spread as 50%. The heating season is considered from October to April, according to the Italian Legislative decree 412/93 [78]. The calculation of the energy demand for space heating is based on the definition of temperature set points equal to 21°C for the occupied hours (9 am – 5 pm) during the winter season, switching to a constant value equal to 18°C during the night and weekend days, to be closer to the real operation. The setpoint temperature for the cooling season is set at 26°C and 60% relative humidity during the occupied hours, while it increases to 28°C during non-occupied periods (8 am-9 am and 5 pm-6 pm). The envelope

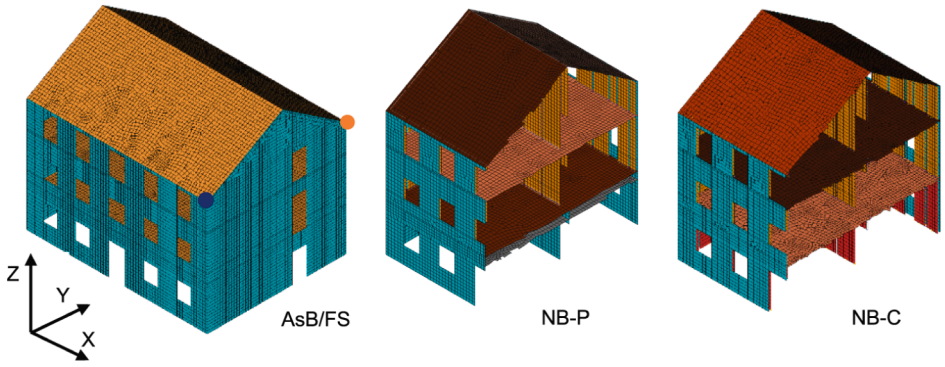

Fig. 3. Finite element models per each configuration (NB-P and NB-C models were sectioned to allow the view of inner part). Control points considered for the calculation of capacity curves are marked in blue and orange, for X and Y directions, respectively. (For interpretation of the references to colour in this figure legend, the reader is referred to the web version of this article.)

Table 6
Mechanical properties of CLT panels (x: in-plane, parallel to outer grains; y: in-plane, orthogonal to outer grains; z: out-of-plane).

CLT Panel	Structural function	Thickness [mm]	E_x [MPa]	E_y [MPa]	E_z [MPa]	G_{xy}, G_{xz}, G_{zy} [MPa]
3-Layer	Wall, Roof	100	7667	5250	417	690
5-Layer	Diaphragm	140	9047	3869	417	690

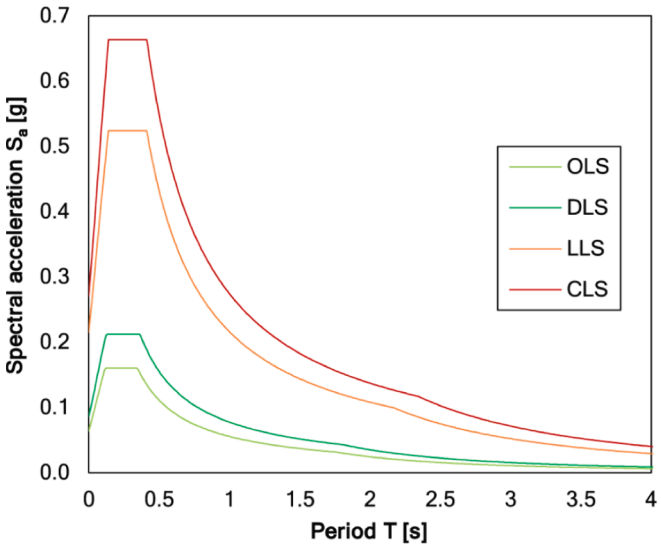

Fig. 4. Smooth seismic spectra for OLS, DLS, LSLS and CLS according to [34].

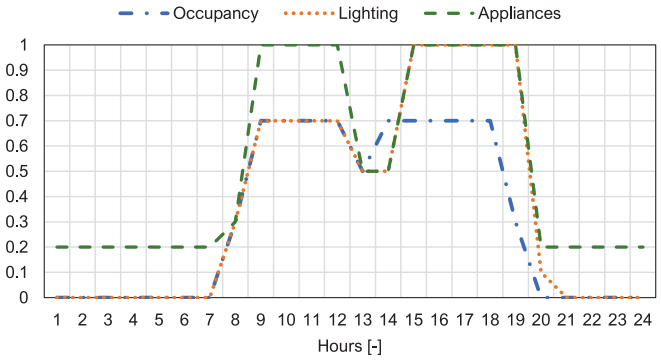

Fig. 5. Schedules of internal loads.

stratigraphy implemented in the model was defined based on the information collected from historic documents. Material properties were adopted according to UNI 11552 Standard [79]. The oldest parts of the building, made of massive stone masonry, have a high thermal inertia that can be exploited to optimize the operating condition of the system, since a significantly high thermal capacity may influence the operative temperature of the thermal zones and, consequently, the overall energy demand. A vapor barrier was installed between the interior lining and the thermal insulation, as per the typological coupling (or nested building) detail discussed in [23]. This positioning prevents moisture migration into the EPS – masonry interface, where the low vapor permeability of EPS would otherwise increase the risk of interstitial condensation.

For AsB scenario, single glazing windows with thermal transmittance equal to 6 W/(m^2 K) were considered, replaced by a double-glazing low emitting structure (1.4 W/(m^2 K)) in the area of intervention (ER, NBb and NB). Similarly, different values of air change rates were associated with the selected scenarios due to the combination of the coupled CLT-URM wall structure and replacement of windows openings (0.7 h^{-1} for AsB, 0.5 h^{-1} for ER and NBb, 0.2 h^{-1} for NB).

Moreover, primary energy use was calculated comparing various combinations of generation systems for space heating and cooling. Case A represents the energy consumption of the building assuming to maintain the generation system, a traditional gas boiler ($\eta = 0.8$). Case B implies the replacement of the system with a condensing gas boiler (maintaining the emission system, thus existing high temperature radiators, $\eta = 0.9$) with a split air conditioner for space cooling. Case C includes the replacement of radiators with radiant systems or fan coils to support the installation of a heat pump (based on the datasheets of real heat pumps, seasonal values have been considered: COP = 3.6 and EER = 4.2) [80].

3. Results and discussion

The results of structural analyses and thermal simulations are discussed in this Section.

3.1. Structural and seismic behavior

The assessment of the structural intervention is performed by comparison among the various layouts, AsB, FS, NB-P, NB-C. Nonlinear static analyses were performed, according to [34,57], along the two main horizontal directions, longitudinal (X) and transverse (Y), and according to uniform mass load distribution.

The outcomes of pushover analyses are presented in terms of equivalent horizontal acceleration, i.e., base shear V on weight W, and global roof-drift (i.e., ratio of top horizontal displacement d to building height h), as per [75]. Fig. 6 shows the capacities curves for AsB, FS, NB-P, NB-C, distinguished for LB and UB property sets. For the sake of clarity, the layout codes are merged with the set codes in the following to enable a straightforward identification (e.g., NB-C-LB).

For LB sets, the curves showed a rather brittle behavior, without a clear post-peak phase. Such behavior is likely to occur in FE models of historical masonry structures with scarce mechanical properties [49,55,81]. Thanks to the mechanical compatibility of timber retrofit with masonry, the variation of initial stiffness is limited for the four layouts, in accordance with experimental investigations described in Table 1.

The FS-LB layout enhanced the capacity compared to the AsB-LB configuration, primarily due to the box-like behavior and mass reduction provided by the CLT floors. Higher acceleration load capacities were achieved in both NB-P-LB and NB-C-LB cases, while a significant increase in drift capacity was observed only in the latter. Concerning UB set, the beneficial effect of NB-C-UB in terms of load capacity is evident, although a reduction of displacement capacity was noticed. The NB-P-UB model confirmed the benefits of the Nested Building intervention also in its partial configuration, providing an improved capacity comparable to FS-UB intervention.

Capacities in terms of Peak Ground Acceleration (PGA) were calculated for AsB, FS, NB-P and NB-C, to compare the analyzed configurations for incremental limit states (Fig. 7). Indeed, the variation in capacity values can help to understand the structural benefits of interventions. The capacity PGA progressively increased with incremental retrofits introduced. The introduction of FS had a beneficial effect compared to AsB, since effective floor diaphragms were introduced, and box behavior developed. In this way, the resisting mechanism of X-direction piers were exploited, thus increasing the seismic capacity along X direction compared to Y. Such hierarchy was kept for all retrofit strategies. The improvements provided by FS and NB-P are comparable,

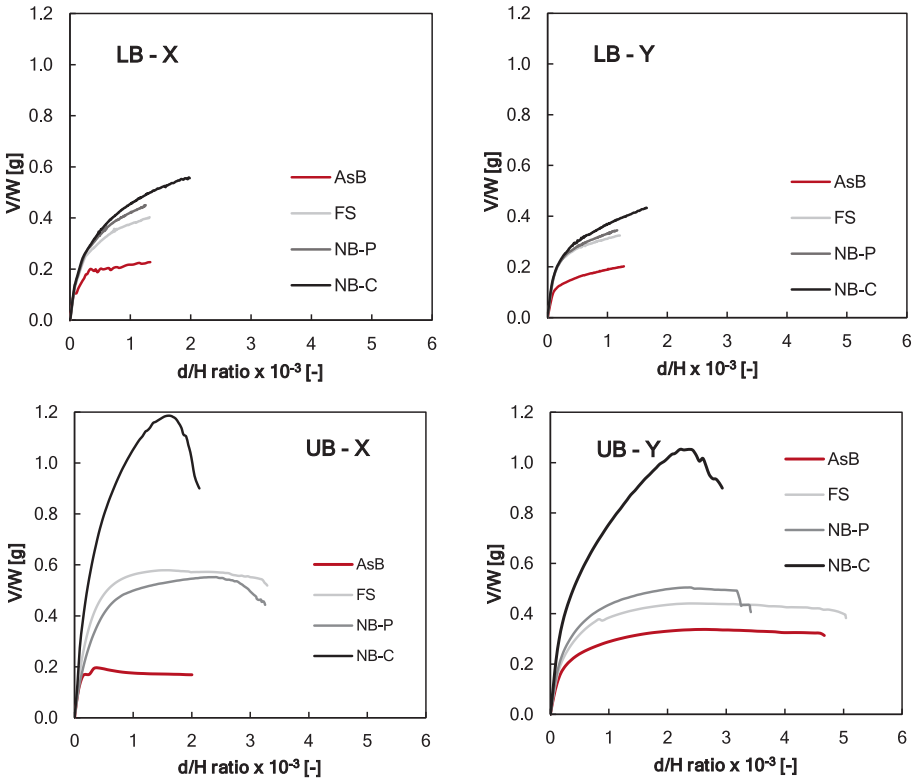

Fig. 6. Capacity curves for LB (up) and UB (down) sets, according to X (left) and Y (right) load directions.

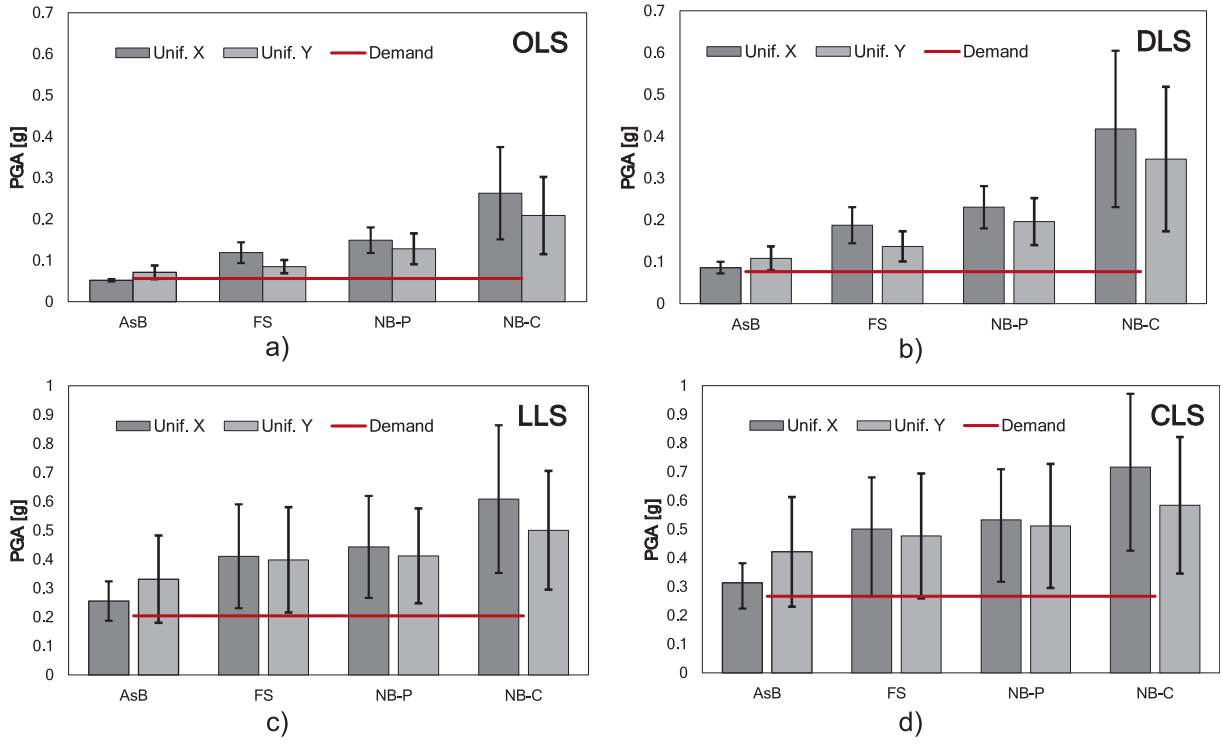

Fig. 7. Bar charts of average capacity PGA, with indication of LB and UB, for a) OLS, b) DLS, c) LLS, d) CLS limit states.

although for the LB set the latter capacities were always higher. However, it should be noted that FS had a stiff plane at roof eave level, whereas NB-P did not (Fig. 1).

The most significant improvement was observed in the NB-C intervention. Considering the site PGA demand, both NB-P and NB-C layouts at the LB provided sufficient seismic capacity for the LLS and CLS, whereas the FS layout remained insufficient.

Understanding how the NB approach enhances the performance of the analyzed URM structure is of particular interest. Fig. 8 compares tensile principal strains (E1) in the main façades, at CLS. While in the

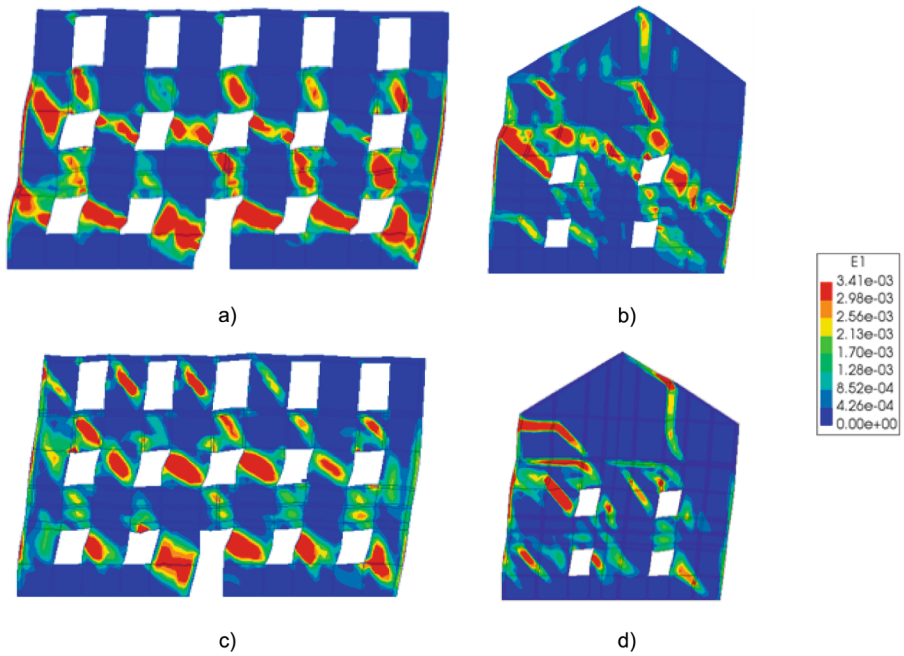

Fig. 8. Ultimate tensile strain diagram for Uniform X and Y load pattern, in the a, b) AsB and c,d) NB models.

AsB layout (Fig. 8a,b) strains are lumped at first and (partly) at second story, NB (Fig. 8c,d) induces strains spread among all stories. In addition, AsB shows strains distributed indistinctly to piers and lintels, whereas in NB strains are concentrated within piers, with lintels undergoing only minor deformations. This is one of the mechanisms by which the seismic behavior of the building is improved through NB intervention, and it is an extension of what was found at pier scale [31,32], where a diffuse distribution of cracks in the coupled CLT-URM walls was recorded.

The contribution of the endoskeleton to the seismic performance of the structure, as a function of the damage sustained by the masonry envelope, is detailed in Appendix B. The timber components carry only a minor portion of the seismic shear forces until damage occurs in the masonry, resulting in only a limited variation in the initial stiffness of the structure. Forces underwent by endoskeleton brackets were found to be all below the characteristic and design yielding limits, so that the CLT nest appeared almost undamaged by the seismic event at CLS, as per preliminary structural design.

3.2. Energy performance

The outcomes of dynamic analyses performed with EnergyPlus, carried out for each combination presented in Table 2, are reported in this Section. Results of the baseline case AsB are compared with similar outcomes of Geo4Civhic [82,83], as well as with the WebTool provided by the project TABULA [84]. Table 7 provides the specific energy demand for space heating and cooling per floor (F0 is the ground floor, F1 is the first floor, F2 is the second floor), as well as the energy saving compared to the AsB baseline case (in brackets). As a general trend, comparable results were obtained for energy retrofit (ER) – EPS insulation within an insulated wall lining system – and bare Nested Building (NBb) scenarios – use of timber endoskeleton without specific thermal insulation, for both Partial and Complete interventions. Hence, the application of the timber structure can be considered beneficial also from an energy point of view.

The energy demand for the ground floor F0 was slightly higher for the NBb-P scenario compared to the AsB. This is most likely due to the presence of timber in the floor of F2, which resulted in the slab thermal mass being heated primarily by thermal energy from F0. Moreover, heat losses at the slab-wall interface had a greater impact on the heating demand of F0. Using EPS insulation within an insulated wall lining system (ER) reduced heating energy demand by 10% to 15%, compared to the timber skeleton alone (NBb), for F1 and F2. The latter allowed a reduction in energy consumption between 35% and 38% compared to AsB scenario. A similar performance was seen also for the cooling energy demand. Looking at NBb-C, the same trend was maintained; however,

Table 7
Se (F0 = ground floor, F1 = first floor, F2 = second floor).

	Floor	AsB	Partial intervention			Complete intervention		
			ER-P	NBb-P	NB-P	ER-C	NBb-C	NB-C
Space heating [kWh/m^2]	**F0**	55.0	58.4 (+6%)	60.2 (+9%)	58.2 (+6%)	20.9 (−62%)	26.8 (−51%)	11.7 (−81%)
	F1	56.2	28.9 (−48%)	34.8 (−38%)	14.7 (−74%)	26.7 (−52%)	33.7 (−40%)	17.7 (−49%)
	F2	55.7	27.6 (−50%)	36.0 (−35%)	16.3 (−71%)	27.2 (−51%)	35.9 (−36%)	16.4 (−54%)
Space cooling [kWh/m^2]	**F0**	5.2	4.3 (−19%)	4.2 (−20%)	4.1 (−21%)	2.9 (−45%)	2.9 (−45%)	2.4 (−54%)
	F1	14.6	9.9 (−32%)	11.3 (−22%)	11.5 (−21%)	9.2 (−37%)	11.0 (−25%)	10.7 (−26%)
	F2	13.6	8.8 (−35%)	9.8 (−28%)	9.9 (−27%)	8.6 (−7%)	9.7 (−29%)	9.8 (−28%)

the additional retrofit of F0 increased the energy saving both in summer and winter.

In the case study, the adoption of a 10 cm EPS insulation layer leads to a substantial reduction in energy demand (Case ER-C, from 51 to 62%), indicating that transmission losses through the opaque envelope – a primary driver of the building energy demand – are already significantly reduced. Further increases in insulation thickness primarily target this component, while their impact on the overall energy demand becomes progressively smaller as other factors, as ventilation and infiltration losses, solar and internal gains, and system efficiencies, become increasingly dominant in the energy balance. Hence, the proposed integrated solution, which combines traditional insulation with a timber endoskeleton, emerges as the most effective strategy for reducing energy demand; it maximizes energy savings while providing further benefits inherent to integrated interventions. However, even the timber skeleton alone – without additional insulation – yields a measurable enhancement in thermal and energy performance. Although it does not deliver the optimal thermal performance, it still offers a significant energy savings benefit while enhancing economic, environmental and social sustainability [19].

Fig. 9 represents the indoor operative temperatures of F1 for a typical winter week, in function of the simulated scenarios. The lowest trend was obtained for AsB (i.e., without insulated envelope). The highest indoor temperature, thus potentially better indoor comfort and lower energy consumption, was obtained with integrated NB (both Partial and Complete), which combined structural layer and thermal insulation. This impact was more pronounced during the weekend, characterized by free-running operations (i.e., when the HVAC system is not operating). During the winter season, ER and NBb showed an intermediate behavior in terms of operative temperatures between AsB and NB, because of the lower envelope losses achieved either with the dedicated thermal insulation (ER) or the wooden endoskeleton (NBb). Results confirmed the findings of Kang et al. [45], with indoor temperature increments of more than 1°C.

Considering a typical summer week (Fig. 10), AsB still exhibits the least desirable behavior, reaching temperatures up to 32°C. Regardless of the retrofit scenario considered –thermal insulation (ER), timber endoskeleton (NBb), or their combination (NB) – the indoor temperature decreases by approximately 1–2°C compared to the existing condition. Thanks to the low thermal transmittance of the applied insulation, the effect of retrofit actions both on temperatures and energy reduction was most beneficial during the winter, which is the dominant season due to the altitude of the location (≈1000 m MSL) and consequent cold to mild climate.

Table 8 lists the primary energy values estimated for A (traditional gas boiler), B (condensing gas boiler), C (heat pump) cases of generation systems, as described in Section 3.3. The best scenario is NB-C combined with Case C (i.e., heat pump), with a 67% primary energy saving compared to the baseline case (AsB, Case A).

Comparing the energy use resulting from the simulations of NBb and ER with AsB, shows that both strategies achieve similar improvements in energy performance. This indicates that the wooden endoskeleton alone (NBb) already provides a significant added value, nearly halving energy consumption when the integrated structural–energy retrofit (NBb-C) is applied compared to the AsB case.

4. Conclusions

This paper evaluated the capability of the *Nested Building* approach to integrate seismic, energy, and functional retrofit at full building scale. Several layouts were examined, beginning with the replacement of existing clay-block and RC-joist floors with timber alternatives, followed by the construction of a partial endoskeleton at the second and third stories, and culminating in the assembly of a complete endoskeleton. The outcomes of the structural and energy simulations conducted on the pilot-case support the effectiveness of this integrated technique, leading to the following generalized conclusions:

- Timber-based integrated interventions do not significantly alter the URM structure initial stiffness, as the endoskeleton contribution becomes active during the nonlinear phase of the masonry response, when URM walls stiffness decreases due to cumulative damage.
- The Complete Nested Building (NB-C) layout proves to be the most effective integrated strategy, offering the highest structural and seismic improvements while reducing the building primary energy demand to approximately one-third of the baseline case (As-Built).
- Partial applications of the intervention also deliver meaningful improvements in both seismic and energy performance. While the partial energy retrofit (ER-P) offers higher energy savings (48%), the partial bare Nested Building solution (NBb-P) provides a comparable reduction (38%) along with enhanced seismic performance – particularly beneficial in cases of poor masonry quality.
- Structural improvements in NB-P and NB-C configurations are attributed to the endoskeleton capacity to redistribute tensile strains across all stories, preventing their concentration at the lower stories and promoting strain localization within piers rather than lintels.
- The CLT endoskeleton whether applied alone (NBb) or combined with dedicated thermal insulation (NB) enhances indoor environmental conditions, raising winter operative temperatures by 1°C to 3°C (depending on the operational schedule), and mitigating summer overheating by reducing peak indoor temperatures by approximately 1°C to 2°C.
- Even without dedicated thermal insulation, the bare application of the timber endoskeleton significantly reduces cooling energy demand, achieving up to 40% savings in the NBb-C scenario. On average, it delivers energy performance only 10–15% lower than that of traditional insulation solutions, demonstrating the inherent efficiency of the proposed strategy.

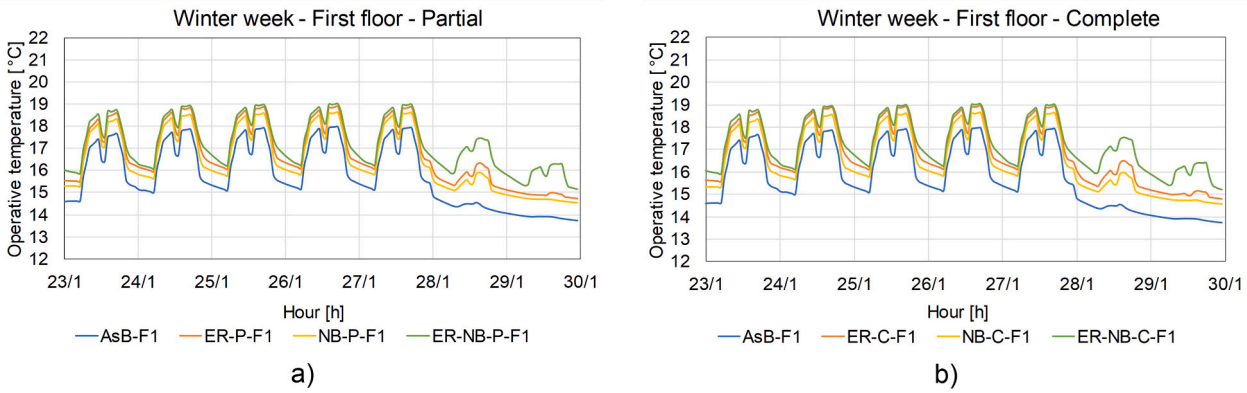

Fig. 9. Indoor operative temperatures of a typical winter week for Partial (a) and Complete (b) scenarios.

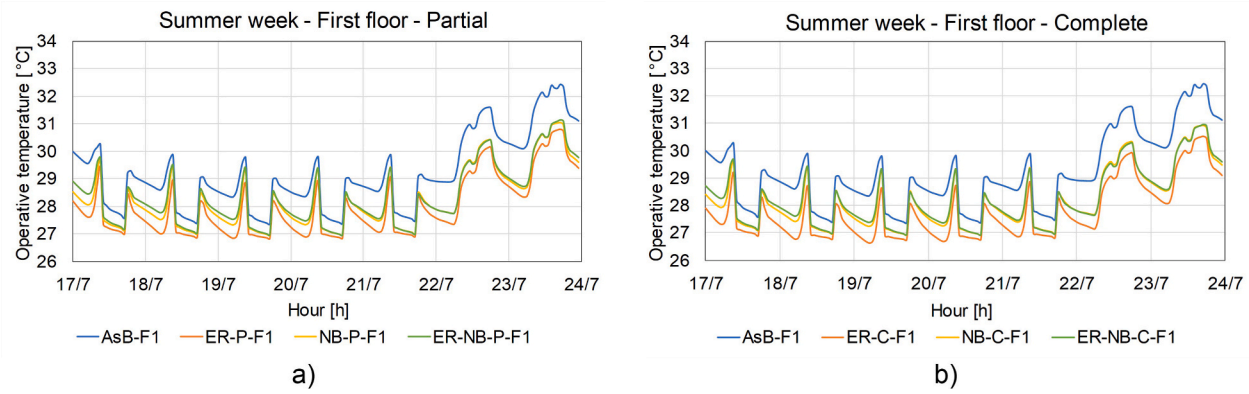

Fig. 10. Indoor operative temperatures of a typical summer week for Partial (a) and Complete (b) scenarios.

Table 8
Primary energy estimation in function of scenarios and generation systems.

	Scenario	Case A	Case B	Case C
		Traditional Gas boiler (no cooling system)	Condensing gas boiler + split air conditioner	Heat pump
Primary energy [kWh/m²]	AsB	96.2	86.7	52.7
	ER-P	66.2	59.7	36.3
	NBb-P	75.2	67.7	41.1
	NB-P	53.8	48.7	29.9
	ER-C	44.9	40.6	24.9
	NBb-C	56.9	51.4	31.4
	NB-C	30.7	28.1	17.5

- The pilot case demonstrates substantial reductions in primary energy for space heating and cooling, with heat pump installation yielding up to 82% energy savings compared to traditional gas boilers.

This paper has demonstrated the potential contribution of the *Nested Building* integrated intervention to the progress of European Union Mission on Adaptation to Climate Change, providing a robust and inclusive pathway towards more resilient and sustainable built environments. This is driven by the principles of the New European Bauhaus – sustainability, aesthetics and inclusion – through a solution which enhances energy efficiency and structural resilience of heritage buildings employing low-carbon materials such as CLT. At the same time, it preserves the aesthetic integrity and cultural value of historic urban environments, including the conservation of the memory of place within local communities. Finally, this integrated approach enables a series of further economic, environmental and social sustainability benefits, which sectorial approaches cannot provide.

Designed to be flexible and adaptable, the strategy can be easily tailored to the specific characteristics and vulnerabilities of different regional building stocks.

CRediT authorship contribution statement

Matteo Salvalaggio: Writing – review & editing, Writing – original draft, Visualization, Validation, Methodology, Investigation, Formal analysis, Data curation, Conceptualization. **Laura Carnieletto:** Writing – review & editing, Writing – original draft, Visualization, Validation, Methodology, Investigation, Formal analysis, Data curation. **Elisa Saler:** Writing – review & editing, Writing – original draft, Formal analysis. **Wilmer Pasut:** Writing – review & editing, Supervision, Funding acquisition. **Umberto Turrini:** Writing – review & editing, Supervision, Conceptualization. **Maria Rosa Valluzzi:** Writing – review & editing, Supervision, Resources, Project administration, Funding acquisition, Conceptualization.

Declaration of competing interest

The authors declare that they have no known competing financial interests or personal relationships that could have appeared to influence the work reported in this paper.

Acknowledgements

The authors wish to thank Eng. M. Pegoraro and Eng. T. Pizziol for their support in the performance of finite element analyses, Mr. E. Bozza, head of Bozza Legnami srl, and SPC Engineering for the collaboration in the executive design of the intervention in the *Cattedra* building.

Funding

This research was funded by the CORE-WOOD (COmpetitive REpositioning of WOOD sector) Italian project, in the framework of POR-FESR 2014–2020 Line 1 Action 1.1.4 of the Veneto Region. Part of the research was also carried out in the framework of the 2022-24 DPC-RELUIS Project (Italian Civil Protection Department - Network of University Labs on Seismic Engineering).

This study was funded also by the European Union - NextGenerationEU, Mission 4, Component 2, in the framework of the GRINS - Growing Resilient, INclusive and Sustainable project (GRINS PE00000018 - CUP H73C22000930001) PE9 - Mission 4, C2, Intervention 1.3., and by the European Union - NextGenerationEU, in the framework of the iNEST - Interconnected Nord-Est Innovation Ecosystem (iNEST ECS_00000043 - CUP H43C22000540006). The views and opinions expressed are solely those of the authors and do not necessarily reflect those of the European Union, nor can the European Union be held responsible for them. This work took place within the framework of the DoE 2023-2027 (MUR, AIS.DIP.ECCELLENZA2023_27.FF project).

Compliance with ethical standards

The authors declare that they have no conflict of interest.

Appendix A

While experimental investigations of URM-timber systems were typically conducted in controlled laboratory settings using contemporary materials, Giongo et al. [31] performed a series of destructive tests on URM specimens cut and isolated within load-bearing walls of an existing and decommissioned building dating back to XIX century (i.e., the Comano Terme bath area in northern Italy). Samples (1.8 x 1.8 m) were made of clay bricks and lime mortar. In case of timber strengthening, two types of fasteners were inserted with pre-drilled holes: type "A" equal to Ø 12 x 180 mm partially threaded screws, type "B" equal to Ø 10 x 230 mm full-threaded screws. Three types of configurations were tested: as-built (bare specimens AsB-1 and −2), repaired (addition of timber panel after testing, RP-1 and −2), retrofitted (addition of timber panel to bare specimen, before test, R3). The number and type of fasteners employed varied according to the respective RP designation. Moreover, for repairing layouts, the connectors position was irregular due to post-test cracks position. R-3 layout had 25B dowels regularly distributed (8 fasteners per m^2) in five rows, with 300 mm spacing. It was proven that the addition of timber element, even as repair tool, allowed to increase the peak bearing load of the panel, with little or no reduction in initial stiffness. However, ultimate displacement capacity was slightly reduced compared to as-built configuration. The retrofitted configuration, instead, offered a consistent load (106 kN on a 75.9 kN maximum for both AsB tests) and displacement increase. The coupling of URM wall with CLT panels resulted in the propagation of damage throughout the pier, thereby enhancing the structural capacity in comparison to the bare specimens, which exhibited the typical diagonal cracks. Riccadonna et al. 2019 [85] performed shear tests on steel connectors to join timber panels with clay brick and stone masonry. Stone exhibited higher load-bearing capabilities than clay brick, despite greater variability due to irregular geometry and consistency. Stone failure resulted from tensile cracks or mortar joint crushing due to weak historical lime mortar. Clay units experienced crushing or splitting failures. Although fasteners choice should have low impact, mild steel ones should be used in case of bricks, due to earlier rise of plastic hinge and better dissipative capacity, while hardened carbon steel fasteners could limit the risk of brittle failure in stone units. Besides, if stone masonry has thick and irregular binder joints, grouted connectors should be considered.

The robustness of FEM strategy for simulating coupled CLT-URM panels was verified by benchmarking numerical outcomes against experimental results. The samples of masonry piers investigated by Giongo et al. [31] were considered, specifically AsB-1 and R-3, for the un-retrofitted and retrofitted configurations.

According to a method already provided in the numerical study by Giongo et al. [54] and replied by the authors [86], the experimental setup was reproduced in DIANA FEA environment [33]. URM pier in AsB-1 and R-3 models were discretized by means of 4-noded linear shell elements (Q20SF element type) with a 50 mm-size mesh, i.e., minor than units size, according to [64].

Properties of URM and connectors were adjusted based on experimental outcomes, starting from values derived by [31] and [85], Italian regulations [57] and [65]. URM parameters (i.e., compressive and tensile strengths, shear retention) were calibrated through the benchmark model of AsB-1 specimen, as listed in Table A.1.

Table A1
Calibrated mechanical characteristics of AsB-1 and R-3 FE models.

Historical clay brick and lime mortar masonry			**60 mm-thick CLT**	
	AsB-1	**R-3**		
E [MPa]	381.2		E_z [MPa]	7700
ν [-]	0.25		E_x [MPa]	3850
f_c [MPa]	1.10		G_{xz} [MPa]	300
G_{fc}[N/mm]	2.96		ρ [kg/m^3]	450
f_t [MPa]	0.03		**Hold-down**	
G_{ft} [N/mm]	0.02	Infinite	k_{tens} [N/mm]	2630
β [-]	0.10		k_{shear} [N/mm]	263
ρ [kg/m^3]	1800		F_{max} [N]	53,000

A sensitivity analysis was performed, varying the compressive and tensile strengths, as well as the shear retention factor. The outcome capacity curves are shown in Fig. A.1a, where the red continuous line correspond to the calibrated model, whose properties are listed in Table A.1. Tensile and shear values were the most influential, as expected since the experimental failure of the specimens occurred by tensile cracking and shear joints separation, with small variations (e.g., β less than 0.2) significantly altering the response. As mentioned in Sub-Section 3.2, this variability was accounted in the modeling of the *Cattedra* pilot case by setting an upper and a lower bound to the URM properties.

Then, the properties of connectors were adjusted simulating the R-3 sample. Based on the fixed set of parameters defined for AsB-1, R-3 was simulated (Fig. A.1c). Linear no-tension interface (L12IFS, 36 elements) was implemented at the base of the CLT panel. Steel connectors were modeled by nodal interfaces (N6IFI) with constitutive shear laws derived by [85], then adjusted by a 0.2 multiplier and addition of a hardening component up to 50 mm displacement (Fig. A.1b), to match the experimental R-3 curve. The results showed an increase in displacement capacity, while the force capacity remained unchanged (Fig. A.1, orange line). This behavior was likely due to the URM insufficient fracture energy, which prevented it from reaching peak force. To investigate this further, the fracture energy was first increased to 0.1 N/mm, and then considered infinite – assuming an ideal elastic–plastic behavior as proposed in [87] (Fig. A.1d, red line).

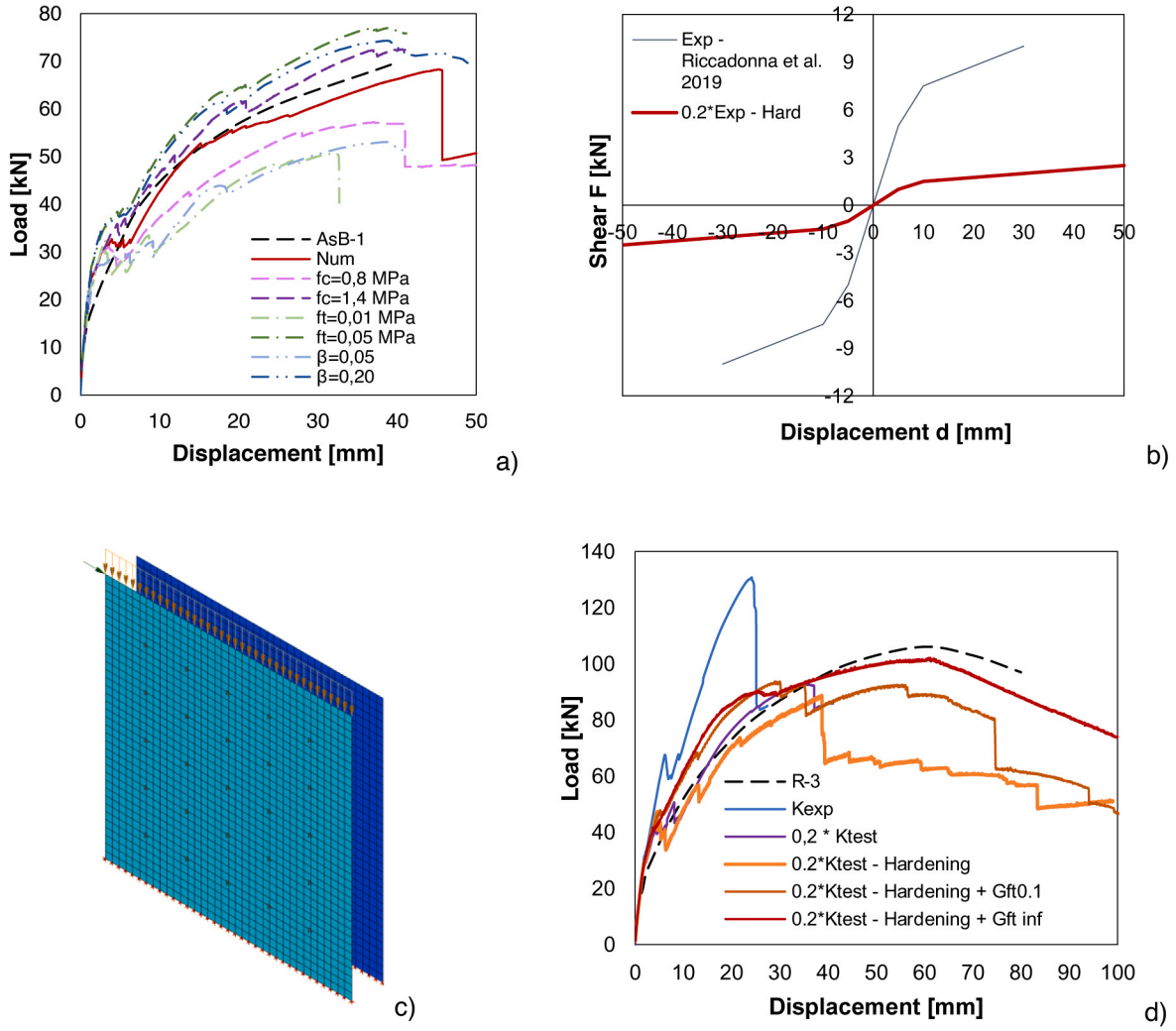

Fig. A1. Numerical benchmark against coupled URM-CLT walls by Giongo et al. 2021 [31]: a) loaddisplacement capacity curves of sensitivity analysis and calibrated curve ('Num') for As-B-1 specimen, b) shear constitutive laws for connectors. c) FE model of URM-CLT coupled wall based on R-3 specimen (URM azure, CLT blue), d) capacity curves of R-3 specimen by scaling of connectors laws and URM tensile fracture energy.

The procedure allowed for two conclusions to be drawn: i) the FE model demonstrated to be capable of reproducing the behavior of URM and coupled URM-CLT walls for the material properties of Table A.1; ii) the effect of connector capacity on the response of the coupled walls may be limited by the tensile capacity of the URM, particularly the fracture energy. Finite values were assumed for the structural models of the case study in order to obtain conservative results to be used in practice design [55,81,88].

Appendix B

The variation in the endoskeleton contribution to the seismic resistance of the structure, as the mass, Young's modulus, and shear modulus of the URM walls vary, is discussed in this Appendix. Analyses were conducted solely for NB intervention and LB set, to limit computational effort. For the same reason, parametric pushover analyses were restricted to the longitudinal direction, assuming a uniform load pattern. Three values were derived from [57] for both Young's modulus ($E_1 = 870$ MPa; $E_2 = 1230$ MPa; $E_3 = 1740$ MPa) and masonry density ($M_1 = 10$ kN/m^3, $M_2 = 15$ kN/m^3, $M_3 = 20$ kN/m^3), resulting in nine combinations.

Fig. B1 illustrates the proportion of base shear absorbed by CLT components (V_{CLT}) relative to the total base shear (V), plotted as a function of V increasing relative to the peak shear load (V_{MAX}). The initial base shear absorbed by the endoskeleton depends on the relative stiffness between URM and CLT, which varies from approximately 10%, (when E is higher) to about 20%, (when E is lower). The ratio between VCLT and V shear showed a flex point occurring between 8% and 15% of peak shear load of the structure. The URM mass influences this behavior: greater mass tends to shift the flex point toward higher load levels. For mass values M1 and M2, the percentage increase in CLT shear contribution between these phases slightly grows as the elastic modulus increases. However, no clear trend was observed for M3. Beyond the flex point, the contribution of the endoskeleton increases approximately linearly. These findings demonstrate that the NB can effectively support the refurbishment of existing buildings, providing structural enhancement that is proportional to the URM quality (i.e., stiffness).

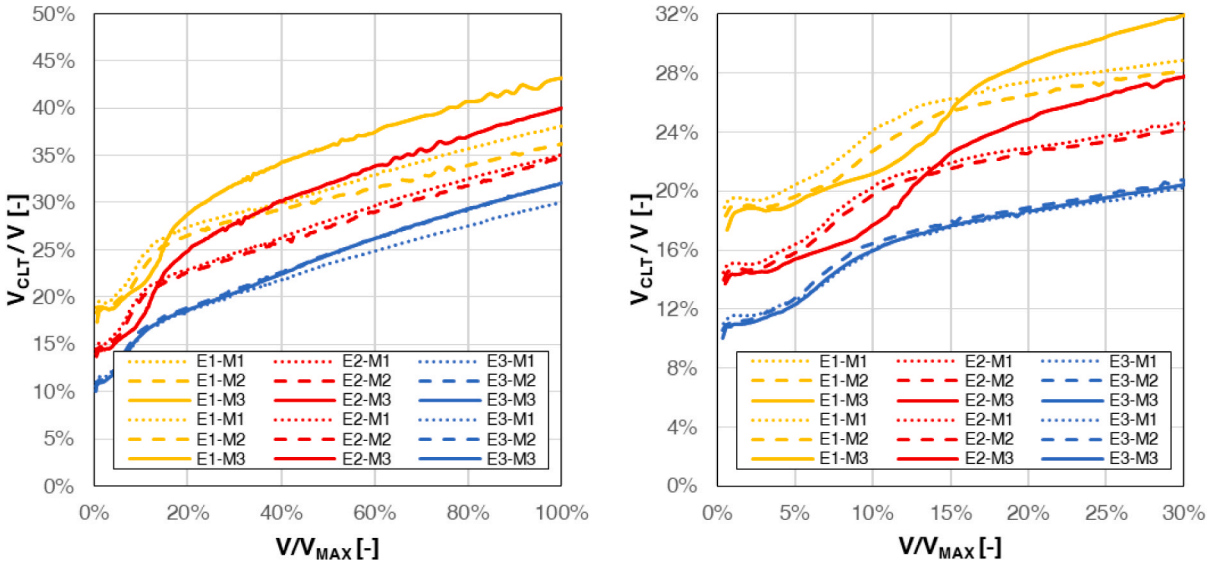

Fig. B1. Endoskeleton shear load in function of overall shear load increasing to ultimate V_{MAX}.

Data availability

Data will be made available on request.

References

[1] A. Gevorgian, S. Pezzutto, S. Zambotti, S. Croce, U.F. Oberegger, R. Lollini, L. Kranzl, A. Müller, European Building Stock Analysis. A country by country descriptive and comparative analysis of the energy performance of buildings, 2021.

[2] D.A. Pohoryles, C. Maduta, D.A. Bournas, L.A. Kouris, Energy performance of existing residential buildings in Europe: a novel approach combining energy with seismic retrofitting, Energ. Build. 223 (2020) 110024, https://doi.org/10.1016/j.enbuild.2020.110024.

[3] Legge 9 Gennaio 1991, n.10 - Norme per l'attuazione del Piano energetico nazionale in materia di uso nazionale dell'energia, di risparmio energetico e di sviluppo delle fonti rinnovabili di energia, (1991).

[4] A. Caprino, F. Lorenzoni, L. Carnieletto, L. Feletto, M. De Carli, F. da Porto, Integrated seismic and energy retrofit interventions on a urm masonry building: the case study of the former courthouse in fabriano, Sustainability (Switzerland) 13 (2021), https://doi.org/10.3390/su13179592.

[5] C. Modena, M.R. Valluzzi, F. da Porto, F. Casarin, Structural aspects of the conservation of historic masonry constructions in seismic areas: remedial measures and emergency actions, Int. J. Architectural Heritage 5 (2011) 539–558, https://doi.org/10.1080/15583058.2011.569632.

[6] M.R. Valluzzi, L. Sbrogiò, Y. Saretta, H. Wenliuhan, Seismic response of masonry buildings in historical centres struck by the 2016 central italy earthquake. Impact of building features on damage evaluation, Int. J. Architectural Heritage (2021), https://doi.org/10.1080/15583058.2021.1916852.

[7] L. Sbrogiò, Y. Saretta, M.R. Valluzzi, Empirical performance levels of strengthened masonry buildings struck by the 2016 central italy earthquake: proposal of a new taxonomy, Int. J. Architectural Heritage (2022), https://doi.org/10.1080/15583058.2021.2011474.

[8] M. Hemmati, T. Messadi, H. Gu, Life cycle assessment of cross-laminated timber transportation from three origin points, Sustainability (Switzerland) 14 (2022), https://doi.org/10.3390/su14010336.

[9] The European Parliament and the Council, Directive 2018/844 of 30 May 2018 amending Directive 2010/31/EU on the energy performance of buildings and Directive 2012/27/EU on energy efficiency, 2018.

[10] L. Giresini, F. Graziotti, G. Guerrini, Multicriteria decision tools for selection of sustainable integrated retrofits: application to the seismic and energy upgrade of a masonry building, J. Build. Eng. 95 (2024) 110017, https://doi.org/10.1016/j.jobe.2024.110017.

[11] D.A. Bournas, Concurrent seismic and energy retrofitting of RC and masonry building envelopes using inorganic textile-based composites combined with insulation materials: a new concept, Compos. B Eng. 148 (2018) 166–179, https://doi.org/10.1016/j.compositesb.2018.04.002.

[12] T.C. Gkournelos, D. P., Bournas, D. A., Triantafillou, Combined seismic and energy upgrading of existing buildings using advanced materials, 2019. https://doi.org/10.2760/17376.

[13] A. Borri, M. Corradi, R. Sisti, C. Buratti, E. Belloni, E. Moretti, Masonry wall panels retrofitted with thermal-insulating GFRP-reinforced jacketing, Mater. Struct. 49 (2016) 3957–3968, https://doi.org/10.1617/s11527-015-0766-4.

[14] T.C. Triantafillou, K. Karlos, P. Kapsalis, L. Georgiou, Innovative structural and energy retrofitting system for masonry walls using textile reinforced mortars combined with thermal insulation: in-plane mechanical behavior, J. Compos. Constr. 22 (2018), https://doi.org/10.1061/(ASCE)CC.1943-5614.0000869.

[15] J. Zanni, S. Cademartori, A. Marini, A. Belleri, C. Passoni, E. Giuriani, P. Riva, B. Angi, G. Brumana, A.L. Marchetti, Integrated deep renovation of existing buildings with prefabricated shell exoskeleton, Sustainability (Switzerland) 13 (2021) 1–27, https://doi.org/10.3390/su132011287.

[16] V. Manfredi, A. Masi, Seismic strengthening and energy efficiency: towards an integrated approach for the rehabilitation of existing RC buildings, Buildings 8 (2018) 36, https://doi.org/10.3390/buildings8030036.

[17] A. Marini, C. Passoni, A. Belleri, F. Feroldi, M. Preti, G. Metelli, P. Riva, E. Giuriani, G. Plizzari, Combining seismic retrofit with energy refurbishment for the sustainable renovation of RC buildings: a proof of concept, Eur. J. Environ. Civ. Eng. (2017) 1–21, https://doi.org/10.1080/19648189.2017.1363665.

[18] S. Labò, C. Passoni, A. Marini, A. Belleri, Design of diagrid exoskeletons for the retrofit of existing RC buildings, Eng. Struct. 220 (2020) 110899, https://doi.org/10.1016/j.engstruct.2020.110899.

[19] C. Passoni, M. Caruso, L. Felicioni, P. Negro, The evolution of sustainable renovation of existing buildings: from integrated seismic and environmental retrofitting strategies to a life cycle thinking approach, Bull. Earthquake Eng. 22 (2024) 6327–6357, https://doi.org/10.1007/s10518-024-01991-0.

[20] L. Penazzato, R. Illampas, D.V. Oliveira, The challenge of integrating seismic and energy retrofitting of buildings: an opportunity for sustainable materials? Sustainability 16 (2024) 3465, https://doi.org/10.3390/su16083465.

[21] M. Salvalaggio, M.R. Valluzzi, Optimization of intervention strategies for masonry buildings based on CLT components, Heritage 5 (2022) 2142–2159, https://doi.org/10.3390/heritage5030112.

[22] D. Malomo, Y. Xie, G. Doudak, Unified life-cycle cost–benefit analysis framework and critical review for sustainable retrofit of Canada's existing buildings using mass timber, Can. J. Civ. Eng. 51 (2024) 687–703, https://doi.org/10.1139/cjce-2023-0222.

[23] G. Iovane, A. Sandoli, D. Marranzini, R. Landolfo, A. Prota, B. Faggiano, Timber based systems for the seismic and energetic retrofit of existing structures, Procedia Struct. Integrity 44 (2023) 1870–1876, https://doi.org/10.1016/j.prostr.2023.01.239.

[24] M.R. Valluzzi, E. Saler, A. Vignato, M. Salvalaggio, G. Croatto, G. Dorigatti, U. Turrini, Nested buildings: an innovative strategy for the integrated seismic and energy retrofit of existing masonry buildings with CLT panels, Sustainability (switzerland) 13 (2021) 1–19, https://doi.org/10.3390/su13031188.

[25] N. Ademovic, A. Formisano, L. Penazzato, D.V. Oliveira, Seismic and energy integrated retrofit of buildings: a critical review, Front. Built Environ. 8 (2022) 963337, https://doi.org/10.3389/fbuil.2022.963337.

[26] G. Frunzio, S. Rinaldi, M. Guadagnuolo, L. Massaro, L. Di Gennaro, USE OF ENGINEERED WOOD FOR THE RETROFITTING OF EXISTING STRUCTURES, in: Lisbon, Portugal, 2022: pp. 225–236. https://doi.org/10.2495/ARC220191.

[27] N. Damiani, M. Miglietta, G. Guerrini, F. Graziotti, Numerical Assessment of the seismic performance of a timber retrofit solution for unreinforced masonry buildings, Int. J. Architectural Heritage 17 (2023) 114–133, https://doi.org/10.1080/15583058.2022.2106461.

[28] G. Guerrini, N. Damiani, M. Miglietta, F. Graziotti, Experimental validation of analytical equations for retrofitting masonry buildings with timber frames and boards, Eng. Struct. 300 (2024) 117124, https://doi.org/10.1016/j.engstruct.2023.117124.
[29] D. Cassol, M. Danovska, A. Prada, I. Giongo, Timber-based strategies for seismic collapse prevention and energy performance improvement in masonry buildings, Sustainability 16 (2024) 392, https://doi.org/10.3390/su16010392.
[30] J. Liu, M. El-Assaly, W. Garcia Mendez, B. Pulatsu, D. Chung, P. Tidwell, D. Malomo, A low-cost timber cladding system for the sustainable retrofit of masonry buildings: mechanical characterization under diagonal compression, Eng. Struct. 322 (2025) 119099, https://doi.org/10.1016/j.engstruct.2024.119099.
[31] I. Giongo, E. Rizzi, D. Riccadonna, M. Piazza, On-site testing of masonry shear walls strengthened with timber panels, Proceedings of the Institution of Civil Engineers: Structures and Buildings 174 (2021) 389–402. https://doi.org/10.1680/jstbu.19.00179.
[32] L. Pozza, L. Marchi, D. Trutalli, R. Scotta, In-plane strengthening of masonry buildings with timber panels, Proceedings of the Institution of Civil Engineers - Structures and Buildings (2021) 1–15. https://doi.org/10.1680/jstbu.19.00121.
[33] DIANA FEA 10.4, (2020).
[34] Ministero delle Infrastrutture e dei Trasporti, Decreto Ministeriale 17 Gennaio 2018 - Aggiornamento delle "Norme Tecniche Per le Costruzioni," Italy, 2018.
[35] EnergyPlus, (2023). https://energyplus.net/ (accessed February 15, 2024).
[36] OpenStudio, (2024). https://www.openstudio.net/.
[37] I. Sustersic, B. Dujic, Seismic Strengthening of Existing Concrete and Masonry Buildings with Crosslam Timber Panels, Materials and Joints in Timber Structures: Recent Developments of Technology. RILEM Bookseries 9 (2014) 713–723. https://doi.org/10.1007/978-94-007-7811-5.
[38] L. Pozza, F. Evangelista, R. Scotta, CLT used as seismic strengthener for existing masonry walls, in: XVII Convegno ANIDIS "L'Ingegneria Sismica in Italia". Pistoia, 17 - 21 Settembre 2017, 2017: pp. 210–220.
[39] A. Borri, R. Sisti, M. Corradi, Seismic retrofit of stone walls with timber panels and steel wire ropes, in: Proceedings of the Institution of Civil Engineers: Structures and Buildings 174, 2021, pp. 359–371, https://doi.org/10.1680/jstbu.19.00100.
[40] G. Guerrini, N. Damiani, M. Miglietta, F. Graziotti, Cyclic response of masonry piers retrofitted with timber frames and boards, Proceedings of the Institution of Civil Engineers - Structures and Buildings (2021) 1–17. https://doi.org/10.1680/jstbu.19.00134.
[41] E. Rizzi, I. Giongo, D. Riccadonna, M. Piazza, Testing of Irregular Stone Masonry Strengthened with Cross-Laminated Timber, Lecture Notes in Civil Engineering 209 LNCE (2022) 1008–1017. https://doi.org/10.1007/978-3-030-90788-4_78.
[42] F. Ascione, N. Bianco, G. Maria Mauro, D.F. Napolitano, Building envelope design: Multi-objective optimization to minimize energy consumption, global cost and thermal discomfort. Application to different Italian climatic zones, Energy 174 (2019) 359–374. https://doi.org/10.1016/j.energy.2019.02.182.
[43] D. Kumar, M. Alam, P.X.W. Zou, J.G. Sanjayan, R.A. Memon, Comparative analysis of building insulation material properties and performance, Renew. Sustain. Energy Rev. 131 (2020) 110038, https://doi.org/10.1016/j.rser.2020.110038.
[44] B. Shin, S.J. Chang, S. Wi, S. Kim, Estimation of energy demand and greenhouse gas emission reduction effect of cross-laminated timber (CLT) hybrid wall using life cycle assessment for urban residential planning, Renew. Sustain. Energy Rev. 185 (2023) 113604, https://doi.org/10.1016/j.rser.2023.113604.
[45] Y. Kang, H.H. Jo, S. Kim, Enhancing indoor comfort and building energy efficiency with cross-laminated timber (CLT) in hygrothermal environments, J. Build. Eng. 84 (2024) 108582, https://doi.org/10.1016/j.jobe.2024.108582.
[46] M. Adamski, Longitudinal Spiral Recuperators in Ventilation Systems of Healthy Buildings, in: HB 2006 - Healthy Buildings: Creating a Healthy Indoor Environment for People, 2006.
[47] A. Staveckis, A. Borodinecs, Impact of impinging jet ventilation on thermal comfort and indoor air quality in office buildings, Energ. Buildings 235 (2021) 110738, https://doi.org/10.1016/j.enbuild.2021.110738.
[48] K. Myroniuk, Y. Furdas, V. Zhelykh, M. Adamski, O. Gumen, V. Savin, S.-A. Mitoulis, Passive ventilation of residential buildings using the trombe wall, Buildings 14 (2024) 3154, https://doi.org/10.3390/buildings14103154.
[49] N. Gattesco, L. Macorini, In-plane stiffening techniques with nail plates or CFRP strips for timber floors in historical masonry buildings, Constr. Build. Mater. 58 (2014) 64–76, https://doi.org/10.1016/j.conbuildmat.2014.02.010.
[50] S. Cattari, D. Camilletti, A.M. D'Altri, S. Lagomarsino, On the use of continuum Finite Element and Equivalent Frame models for the seismic assessment of masonry walls, J. Build. Eng. 43 (2021) 102519, https://doi.org/10.1016/j.jobe.2021.102519.
[51] A.M. D'Altri, V. Sarhosis, G. Milani, J. Rots, S. Cattari, S. Lagomarsino, E. Sacco, A. Tralli, G. Castellazzi, S. de Miranda, Modeling Strategies for the Computational Analysis of Unreinforced Masonry Structures: Review and Classification, Springer Netherlands, 2020. https://doi.org/10.1007/s11831-019-09351-x.
[52] A. Sandoli, C. D'Ambra, C. Ceraldi, B. Calderoni, A. Prota, Role of perpendicular to grain compression properties on the seismic behaviour of CLT walls, J. Build. Eng. 34 (2021), https://doi.org/10.1016/j.jobe.2020.101889.
[53] I.P. Christovasilis, L. Riparbelli, G. Rinaldin, G. Tamagnone, Methods for practice-oriented linear analysis in seismic design of Cross Laminated Timber buildings, Soil Dyn. Earthq. Eng. 128 (2020) 105869, https://doi.org/10.1016/j.soildyn.2019.105869.
[54] I. Giongo, G. Schiro, M. Piazza, On the Use of Timber-Based Panels for the Seismic Retrofit of Masonry Structures, 3rd International Conference - Protection of Historical Constructions (2017) 12–15.
[55] A. Elyamani, P. Roca, O. Caselles, J. Clapes, Seismic safety assessment of historical structures using updated numerical models: the case of Mallorca cathedral in Spain, Eng. Fail. Anal. 74 (2017) 54–79, https://doi.org/10.1016/j.engfailanal.2016.12.017.
[56] A. Drougkas, P. Roca, C. Molins, Numerical prediction of the behavior, strength and elasticity of masonry in compression, Eng. Struct. 90 (2015) 15–28, https://doi.org/10.1016/j.engstruct.2015.02.011.
[57] Ministero delle Infrastrutture e dei Trasporti, Circolare 21 Gennaio 2019 n.7 - Istruzioni per l'applicazione dell'«Aggiornamento delle "Norme Tecniche Per le Costruzioni"» di cui al Decreto Ministeriale 17 Gennaio 2018 (Italian Guideline), Italy, 2019.
[58] NTC2018, D.M. 17/01/2018. Aggiornamento delle "Norme tecniche per le costruzioni" (in Italian), Official Gazzette of Italian Republic N°42 of 20h February 2018 (2018).
[59] V. Turnsek, F. Cacovic, Some experimental results on the strength of brick masonrywalls, in: 2nd International Brick Masonry Conference, Stoke-on-Trent, 1971: pp. 149–156.
[60] V. Turnsek, P. Sheppard, The shear and flexural resistance of masonry walls, in: International Research Conference on Earthquake Engineering, Skopje, 1980: pp. 517–573.
[61] L. Bejarano-Urrego, E. Verstrynge, G. Giardina, K. Van Balen, Crack growth in masonry: Numerical analysis and sensitivity study for discrete and smeared crack modelling, Eng. Struct. 165 (2018) 471–485, https://doi.org/10.1016/j.engstruct.2018.03.030.
[62] P.B. Lourenço, A. Gaetani, Finite Element Analysis for Building Assessment, Routledge, New York, 2022, 10.1201/9780429341564.
[63] J.G. Rots, Computational Modeling of Concrete Fracture, Delft University of Technology, 1988.
[64] P.B. Lourenço, J.M. Pereira, Seismic Retrofitting Project: Recommendations for Advanced Modeling of Historic Earthen Sites, Getty Conservation Institute; Guimarães, Portugal: TecMinho–University of Minho., Los Angeles, 2018. https://hdl.handle.net/10020/gci_pubs/advanced_modeling.
[65] EN 1995, Eurocode 5: Design of timber structures, Comité Européen de Normalisation, 2014.
[66] EN 1998:2004 + A1, Eurocode 8: Design of structures for earthquake resistance - Part 1: General rules, seismic actions and rules for buildings, 2013.
[67] ETA-11/0086, Three-dimensional nailing plate (Angle brackets and hold-downs for timber-to-timber or timber-to-concrete or steel connections), (2015).
[68] ETA-11/0496, Three-dimensional nailing plate (Angle Bracket for timber-to-timber or timber-to-concrete or steel connections), (2018).
[69] L. Franco, L. Pozza, A. Saetta, M. Savoia, D. Talledo, Strategies for structural modelling of CLT panels under cyclic loading conditions, Eng. Struct. 198 (2019), https://doi.org/10.1016/j.engstruct.2019.109476.
[70] H.J. Blass, P. Fellmoser, Design of solid wood panels with cross layers, in: Proceedings of the 8th World Conference on Timber Engineering 2004, 14-17 June, Lahti, Finland, 2004.
[71] M. Piazza, T. Sartori, SEISMIC-REV - Experimental campaign on Rothoblaas products. Mechanical property investigation via monotonic and cyclic loading, University of Trento, 2015.
[72] M. Salvalaggio, Timber-based Integrated Solutions for the Seismic Improvement of the built Heritage, University of Padova, 2022.
[73] ETA-14/0349, Österreichisches Institut für Bautechnik - OiB Member of EOTA, 2014.
[74] P. Fajfar, P. Gaspersic, The N2 method for the seismic damage analysis of RC buildings, Earthquake Eng. Struct. Dynam. 25 (1996) 31–46, https://doi.org/10.1002/(SICI)1096-9845(199601)25:1%253C31::AID-EQE534%253E3.0.CO;2-V.
[75] J. Milosevic, S. Cattari, R. Bento, Definition of fragility curves through nonlinear static analyses: procedure and application to a mixed masonry-RC building stock, Bull. Earthquake Eng. 18 (2020) 513–545, https://doi.org/10.1007/s10518-019-00694-1.
[76] Comité Européen de Normalisation, EN 16789:2019 - Energy performance of buildings - Ventilation for buildings - Part 1: Indoor environmental input parameters for design and assessment of energy performance of buildings addressing indoor air quality, thermal environment, lighting and acoustics, (2019).
[77] ISO 18523-1:2016 - Energy performance of buildings – Schedule and condition of building, zone and space usage for energy calculation, (2016).
[78] Italian legislative decree n.412/1993, (1993).
[79] UNI/TR 11552:2014 - Abaco delle strutture costituenti l'involucro opaco degli edifici - Parametri termofisici, (2014).
[80] L. Carnieletto, A.D. Bella, D. Quaggiotto, G. Emmi, A. Bernardi, M. De Carli, Potential of GSHP coupled with PV systems for retrofitting urban areas in different European climates based on archetypes definition, Energy Built Environ. 5 (2024) 374–392, https://doi.org/10.1016/j.enbenv.2022.11.005.
[81] F. Clementi, V. Gazzani, M. Poiani, S. Lenci, Assessment of seismic behaviour of heritage masonry buildings using numerical modelling, J. Build. Eng. 8 (2016) 29–47, https://doi.org/10.1016/j.jobe.2016.09.005.
[82] GEO4CIVHIC - Most Easy, Efficient and Low Cost Geothermal Systems for Retrofitting Civil and Historical Buildings, (n.d.). https://ec.europa.eu/inea/en/horizon-2020/projects/h2020-energy/geothermal-energy/geo4civhic.
[83] Cheap-GSHPs Project. Cheap and efficient application of reliable gound source heat exchangers and pumps, (2016).
[84] Institut Wohnen und Umwelt, The joint EPISCOPE and TABULA Website, (2016). https://episcope.eu/welcome/ (accessed February 20, 2005).
[85] D. Riccadonna, I. Giongo, G. Schiro, E. Rizzi, M.A. Parisi, Experimental shear testing of timber-masonry dry connections for the seismic retrofit of unreinforced masonry shear walls, Constr. Build. Mater. 211 (2019) 52–72, https://doi.org/10.1016/j.conbuildmat.2019.03.145.

[86] M. Salvalaggio, M. Pegoraro, E. Saler, U. Turrini, M.R. Valluzzi, Seismic strengthening of existing URM structures through CLT elements: numerical analysis of the application of a novel intervention technique, in: M. Papadrakis, M. Fragiadakis (Eds.), Proceedings of COMPDYN 2021, Athens, Greece, 28-30 June 2021, 2021: pp. 2300–2313. https://doi.org/10.7712/120121.8637.18865.

[87] M. Busselli, D. Cassol, A. Prada, I. Giongo, Timber based integrated techniques to improve energy efficiency and seismic behaviour of existing masonry buildings, Sustainability (Switzerland) 13 (2021), https://doi.org/10.3390/su131810379.

[88] S. Saloustros, L. Pelà, P. Roca, Nonlinear numerical modeling of complex masonry heritage structures considering history-related phenomena in staged construction analysis and material uncertainty in seismic assessment, J. Perform. Constr. Facil 34 (2020) 04020096, https://doi.org/10.1061/(asce)cf.1943-5509.0001494.